NANO LETTERS

2007
Vol. 7, No. 6
1723−1727

Probing in situ the Nucleation and Growth of Gold Nanoparticles by Small-Angle X-ray Scattering

Benjamin Abécassis,[†,§] Fabienne Testard,[†] Olivier Spalla,[*,†] and Philippe Barboux[‡]

LIONS, Service de Chimie Moléculaire, CEA Saclay, Bat. 125, F-91191 Gif-sur-Yvette Cedex, France, and ENSCP, LCAES UMR 7574, F-75005 Paris, France

Received March 27, 2007; Revised Manuscript Received May 11, 2007

ABSTRACT

We probe in situ by synchrotron SAXS/WAXS and UV−visible spectroscopy the nucleation and growth of gold nanoparticles. The use of a fast-mixing stopped-flow device enables the assesment of the whole particle formation process with a 200 ms time resolution. The number of particles, their size distribution, and the yield of the reaction is determined in real time through the quantitative analysis of the SAXS data on an absolute scale. Two ligands exhibit drastically different behaviors: when an alkanoic acid is used, a nucleation phase of 1 s is followed by a growth step whose rate is limited by the reaction of the monomers at the interface; on the other hand, when an alkylamine is used, the nucleation rate is increased by an order of magnitude, thus annealing growth by a lack of monomer and yielding $R = 1$ nm particles in 2 s, as compared with $R = 3.7$ nm in 12 s for the acid case.

In the past few years, control over the size, shape, and composition of inorganic nanocrystals has became far more refined than ever expected,[1−3] and reaction conditions can now be tuned to yield a specific product. However, the predictive character of these essentially empirical approaches remains incomplete, and precisely designed experiments are now necessary to reveal the mechanisms at work in the formation of nanoparticles.[4] During the formation of nanoparticles (NPs), the time and length scales of nucleation and growth processes and their inherent transient nature have hindered the possibility of direct real-time measurements. To date, only a few reliable measurements of the microscopic mechanism and kinetic of nucleation of NP have been made. They often relied either on ex situ microscopy techniques, which can lead to drying artifacts and prevent the time resolution under 1 min, or on indirect techniques, where the size of the particles is deduced from size-dependent optical properties.[5,6] The high brilliance of synchrotron radiation has recently proven useful to probe dynamic phenomenon in nanomaterials.[7,8] Gold nanoparticles (AuNP) are among the oldest and most studied nanoscale materials[9] due to their important potential applications in biotechnology[10] and catalysis.[11] In this paper, we investigate the monophasic synthesis described by Jana et al.[12] The AuNP are obtained through the reduction by a borohydride salt (BH_4^-) of a gold salt solubilized in toluene by a cationic surfactant (DDAB) in the presence of an excess of alkyl derivative ligands, either decylamine or decanoic acid (see Supporting Information). Fast and reproducible mixing of the two precursor solutions (gold salt and reducing agent/ligand solutions) was ensured by the use of a stopped flow device[13−15] (see Supporting Information). The AuNP form in a few seconds and the experimental setup enables the monitoring of their formation from the very beginning of the reaction (dead time of 16 ms) with a time resolution ranging from 3 ms in the case of the UV−visible experiments to 130 ms for the small-angle X-ray scattering (SAXS) and 800 ms for the wide-angle X-ray scattering (WAXS), both performed at the ID02 beamline of the ESRF (European Synchrotron Radiation Facility, Grenoble, France). Figure 1 presents the temporal evolution of the different physical quantities. Time-resolved UV spectrophotometry (Figure 2) allows the different phases of the formation of the AuNP to be checked qualitatively. The gold(III)−DDAB ion pair[16] has a characteristic metal-to-ligand charge-transfer band at $\lambda \simeq 400$ nm. For the acid case, the decrease of the intensity of this peak over 150 ms shows the reduction of Au(III) into Au(I) or Au(0) because none of these complexes absorb in the probed range.

After 150 ms, the UV−visible spectrum is constant during a transient phase of 250 ms. Afterward, starting from $t = 400$ ms, the formation of the AuNP is indicated by the increase of the surface plasmon absorption band ($\lambda_p = 544$

* Corresponding author. E-mail: olivier.spalla@cea.fr.
† LIONS, Service de Chimie Moléculaire.
‡ ENSCP, LCAES UMR 7574.
§ Present adress : LPMCN, Université de Lyon 1 and Physico-Chimie Théorique, ESPCI, Paris, France.

10.1021/nl0707149 CCC: $37.00
Published on Web 05/26/2007

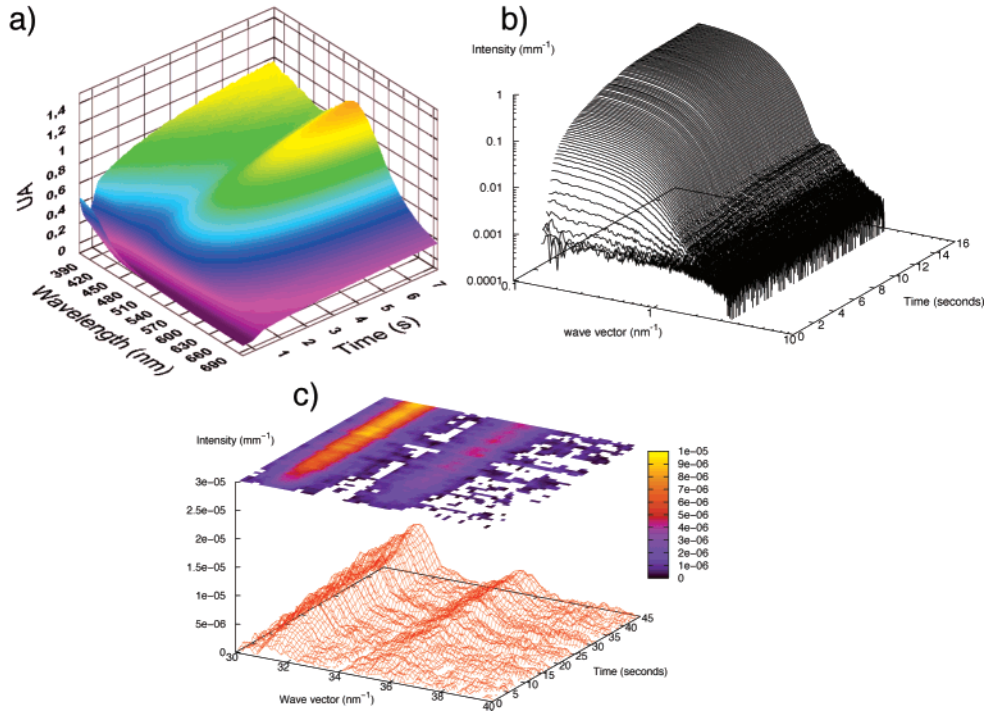

Figure 1. Formation of AuNP by in situ UV−visible, SAXS, and WAXS with the decanoic acid ligand: (a) UV−vis spectrum as a function of time. The decrease of the 400 nm peak in the first instants shows the disappearance of Au(III) before the appearance of the plasmon band at ca. 540 nm. (b) SAXS patterns as a function of time. Just after the mixing and until $t = 140$ ms, the signal is very weak in the whole scattering range, indicating a very low structuration of the solution and the absence of nanoparticles. During the first second, a large increase of the intensity at small q is visible, with a crossover to a rapidly decreasing intensity at large q. As the time of reaction increases beyond 1 s, the intensity at low q continues to develop, while the crossover of regime at large q is reached for a lower q value. In this large q regime, an oscillation is even measurable around 3 nm^{-1}, which is characteristic of the form factor of nanometric objects. This oscillation shifts with time toward lower q, indicating that the scattering objects are growing in size. (c) WAXS patterns as a function of time. The two peaks (110) and (200) are clearly visible, and their intensity increases with time.

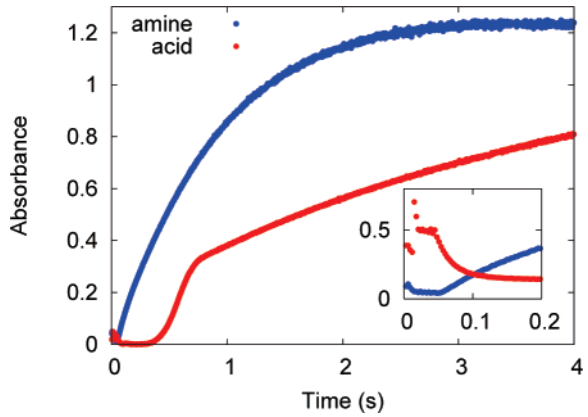

Figure 2. Temporal evolution of UV absorbance at 540 and 400 nm. Absorbance at 540 nm vs time for the two ligands (decanoic acid and decylamine) during AuNP formation. The increase in plasmon intensity presents a break in the acid case, whereas it is much faster and continuous in the amine case. The insert shows the absorbance at 400 nm vs time. For the acid case, the decrease of the signal indicates the reduction of the Au(III) salt. For the amine case, the reduction of the Au(III) salt is not visible: the observed increase after 50 ms is linked to the increase of the plasmon band.

nm) with time. The break around 1 s suggests a change in the regime of formation of the AuNP. When decyl amine is used instead of decanoic acid, the reduction reaction is faster. The disappearance of the Au(III) signal is not visible, and the transient phase is shorter (50 ms). Finally, the plasmon absorption band continuously rises with time, and in contrast to the acid case, only one regime is present. These experiments demonstrate that no Au(III) is present in solution when the AuNP start to nucleate and grow whatever type of ligand and that both the reduction of Au(III) and the formation of the nanoparticles proceed much faster in the case of the amine ligand, showing the strong influence of the nature of the ligand on the kinetic of the formation of AuNP.

Contrary to UV−visible spectrophotometry,[17] SAXS[18,19] is very efficient for assessing unambiguously the number and size distribution of the nuclei and particles during the reaction. Indeed, a solution of atomic gold solely scatters a flat and very weak signal, and after a correct treatment (see Supporting Information), the scattering signal only comes from the contrast between the growing AuNP and the solvent. In that case, the volume fraction Φ of the AuNP can be measured with time using a general property of scattering diagrams (eq 1):

$$\int I(q)q^2\,\mathrm{d}q = 2\pi^2(\Delta\rho)^2\Phi(1-\Phi) \qquad (1)$$

where $\Delta\rho$ is the scattering length density contrast between gold and toluene ($(\Delta\rho)^2 = 1.519 \times 10^{20}$ mm^{-4}). The term

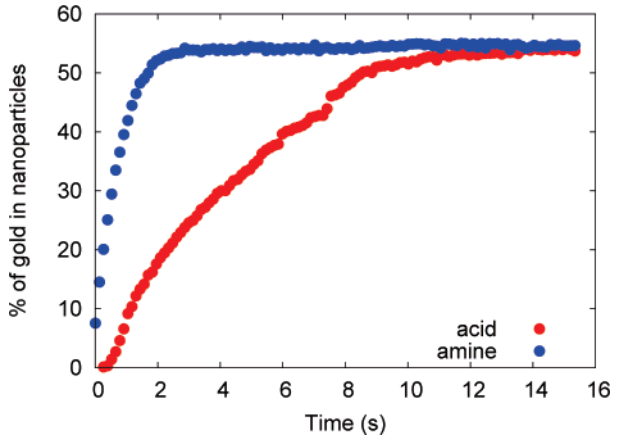

Figure 3. Yield of the reaction as a function of time for the two different ligands obtained via a general property of scattering diagrams.

on the left-hand side is calculated from the experimental scattering diagram, and the term on the right-hand side allows to extract the volume fraction of AuNp in the solution. For a total conversion of atomic gold to nanoparticles, the maximal value of Φ would be $\Phi_{max} = C_0 \times V_m$, where C_0 is the initial concentration of Au(III) and V_m the molecular volume of Au(0) in bulk gold. Thus, the yield of the reaction is obtained at any time t by: $Y = \Phi/\Phi_{max}$, as shown in Figure 3. Two conclusions can be drawn: For the acid case, the reaction lasts 12 s and 53% of gold atoms are transferred to the particles at the end. For the amine case, the final yield is the same but the plateau is reached in 3 s, confirming the fact that the reaction is much faster.

To extract the number density n, the radius r_0, and the polydispersity σ of the nuclei and growing nanoparticles, the scattering from a population of objects is calculated and compared to the SAXS data. The size distribution and number of particles are adjusted to give the best fit using a Levenberg−Marquardt algorithm. In the case of a diluted assembly of spherical particles, the scattered intensity is given by:[20]

$$I(q) = (\Delta\rho)^2 (n \int f(r)V(r)^2P(q,r)\, dr) \qquad (2)$$

where $V(r)$ and $P(q,r) = (9(\sin(qr)-qr\cos(qr))^2)/(qr)^6$ are the volume and the form factor of a sphere of radius r. $f(r)$ is the size distribution function of the particles. The best results were obtained for a population of spheres with a Gaussian size distribution (eq 3):

$$f(r) = \frac{1}{\sqrt{2\pi}\sigma} e^{-[(r-r_0)^2/2\sigma^2]} \qquad (3)$$

The fitting procedure yields a set of 3 paramaters: n, r_0, and σ. The influences of each parameter on the calculated scattering patterns are strongly decoupled, providing unambiguous results for the fitting process. The radius center of the distribution, r_0, and the polydispersity, σ, act on the transition regime of the SAXS pattern where the intensity starts to decrease and on the attenuation of the form factor oscillations at high q. For smaller particles, the plateau at low q will extend over a wider q range, and the scattered intensity will decrease for higher q. The smaller the polydispersity, the sharper the oscillations at high q will be. The number density of particles, n, only acts on the total amplitude as $I(q)$ is directly proportional to n. The agreement of the calculated intensities with the experimental diagrams is almost perfect, as shown in Figure 4 (see also Supporting Information), yielding for every time the size distribution of particles 4c) and providing a solid basis for understanding the time evolution of the different parameters.

The results are shown in Figure 4a for the two different ligands. We observe that the final radius strongly depends on the chemical nature of the ligand (3.5 nm for the acid, 1.4 nm for the amine). Moreover, the kinetics are also different in the first instants of the reaction process. In the acid case, two distinct regimes separated in time can be readily observed. During the first second, there is a rapid increase in the total number of particles, while the average radius remains around 1 nm. This behavior can be ascribed to a nucleation period at the end of which, remarkably, only a very little amount (10 %) of the available gold atoms has been consumed, as can be noticed in Figure 3. Then, after 1.5 s, the number of growing particles remains almost constant while their radius increases by consumption of the remaining atoms in solution, thus defining the growth period. In the amine case, the reaction is faster, and a burst of nucleation with nearly no growth regime is observed. The nucleation rate is simply deduced by dividing the number density of particles at the end of the nucleation period by the time required to generate these stable nuclei. This global value corresponds to an integration over the instantaneous nucleation rate, which strongly depends on the initially increasing supersaturation. A larger nucleation rate is found when amine ligands (1.48×10^{18} $L^{-1}\cdot s^{-1}$) are used instead of acid ligands (5.99×10^{16} $L^{-1}\cdot s^{-1}$). This can be due to a difference in reducing agent activity. For the acid case, the borohydride (a Lewis base) reacts with the carboxylic acid[21] to produce (tri)acyloxyborohydide, a weaker reducing agent, limiting the initial rate of nuclei formation.

The kinetics of growth (only observed with the acid) can either be limited by the diffusion of the monomers toward the surface or by the surface reaction with the monomers.[22,23] In the two limiting cases where one process fully limits the growth, the rate of growth of a particle of radius r is given by a generic differential equation:

$$\frac{dr}{dt} = \upsilon_m A\left(C_0 - n^*\frac{4\pi}{3}r^3 - C_{eq}(\infty)e^{r_{cc}/r}\right) \qquad (4)$$

where $A = K$ in $nm\cdot s^{-1}$ for a surface reaction limited growth and $A = (D/r)$ (D in $nm^2\ s^{-1}$ being the diffusion coefficient of the monomer) for a diffusion-limited growth, $C_{eq}(\infty)$ is the equilibrium solubility of gold with a macroscopic surface, n^* is the number of particles in the solution at the end of the nucleation period, and r_{cc} is the capillary radius, which is linked to the interfacial solid−solvent interfacial tension

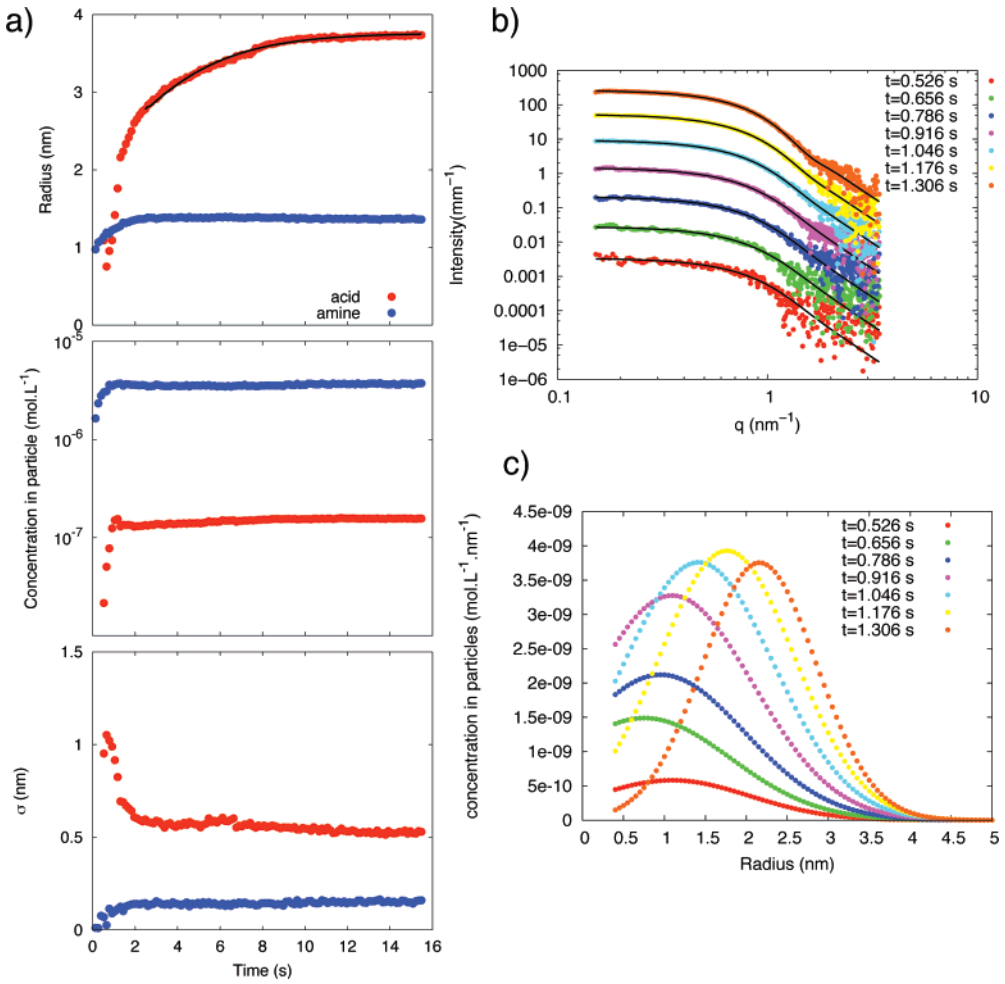

Figure 4. Radius, concentration, and size distribution from SAXS fitting. (a) Results of the fits of the SAXS patterns as a function of time. The concentration of particles (n/N_A), the center of the Gaussian distribution, and the σ parameter are indicated for the two different ligands. (b) SAXS patterns for the first instants of the reaction and the corresponding fits for the case of an acid ligand. (c) Size distribution corresponding to the SAXS patterns in (b).

γ by $r_{cc} = 2\gamma V_m/kT$. The width of the size distribution being small during the whole time of reaction (Figure 4c), eq 4 is integrated versus time by considering a single particle type of size r_0. A good fit is obtained for $A = 2.0 \times 10^4$ nm•s^{-1} and $r_{cc} = 1.2$ nm. A typical particle radius of $r = 2$ nm yields a diffusion coefficient ($D = 4.0 \times 10^4$ nm^2•s^{-1}) 4 orders of magnitude less than a typical diffusion coefficient of any gold complex species in solution. Thus the growth is limited by the surface reaction with a rate constant of $K = 2(\pm 0.5) \times 10^4$ nm•s^{-1}. For the acid case, the end of the nucleation period for a yield of 10% can be explained following Sugimoto's arguments.[22] For a constant feeding of the solution in monomers, Sugimoto established that nucleation stops when the added momomers are all transferred to the growth of the existing particles, suppressing accordingly the chance of nucleating new particles. In the present case, the addition is not constant because it depends on the instantaneous flux of new monomers $Q(t)$. A rate of consumption by growth can also be defined as $Q_G(t) = (dr/dt)•n*(4\pi/\upsilon_m)r^2$. $Q(t)$ goes from a maximum initial value to zero at long time, whereas $Q_G(t)$ increases from 0 at $t = 0$ to a maximum then back to zero at long times. If at any time during the reaction $Q_G(t)$ goes above $Q(t)$, the nucleation will stop. The occurrence of this stoppage intrinsically depends on the instantaneous supersaturation $S(t)$ behavior controlling the size of the first nuclei through $r_c = r_{cc}/\log(S(t))$. This happens for the acid ligand conditions but not for the amine ligand because it does not weaken the reducing agent activity. The final size of the particles is thus controlled by the very first instant of the reaction that these experiments are able to probe: the higher the nucleation rate, the smaller the final particle size. Our results thus unambiguously prove the pionneering hypothesis of Frens.[24]

Finally, the crystalline nature of the AuNP formed is given by the in situ WAXS results. The appearance and growth of two typical diffraction peaks which belong to FCC gold crystal are clearly observed, one at 31.4 nm^{-1} for the (111) plane and the other at 35.5 nm^{-1} for the (200) plane. The full width at half-maximum of the (111) diffraction peak is constant with time and cannot be linked to the size of the particle. On the contrary, the maximum of the (111) peak increases with time with a charateristic behavior. The normalized value (relative to the maximum final value) is superimposed to the normalized radius obtained from SAXS

(see Supporting Information). This indicates that the crystallinity of the particles is not modified during the time of the experiment.

In summary, the quantitative determination of the number density and size distribution has revealed that the ligands determine the final size of gold nanoparticles by controlling their nucleation rate. This opens an effective experimental route toward a comprehensive treatment of the nucleation and growth of nanoparticles.

Acknowledgment. We acknowledge the ESRF for provision of the beam time (proposals SC1523 and SC1923), T. Narayanan for his relevant remarks, and S. Finet for local contact during the experiments on the ID2 beamline. We thank P. Haltebourg and D. Eliott for the conception and building of a specific capillary cell adapted to the stopped flow apparatus. David M. Huang is gratefully acknowledged for careful reading of the manuscript.

Supporting Information Available: Chemicals and synthesis, SAXS/WAXS, stopped-flow, UV−vis, subtraction procedure, SAXS diagrams, diffraction peaks. This material is available free of charge via the Internet at http://pubs.acs.org.

References

(1) Joo, J.; Yu, T.; Kim, Y. W.; Park, H. M.; Wu, F. X.; Zhang, J. Z.; Hyeon, T. *J. Am. Chem. Soc.* **2003**, *125*, 6553−6557.
(2) Park, J.; An, K. J.; Hwang, Y. S.; Park, J. G.; Noh, H. J.; Kim, J. Y.; Park, J. H.; Hwang, N. M.; Hyeon, T. *Nat. Mater.* **2004**, *3*, 891−895.
(3) Manna, L.; Milliron, D. J.; Meisel, A.; Scher, E. C.; Alivisatos, A. P. *Nat. Mater.* **2003**, *2*, 382−385.
(4) Yin, Y.; Alivisatos, P. *Nature* **2005**, *437*, 664−670.
(5) Qu, L. H.; Yu, W. W.; Peng, X. P. *Nano Lett.* **2004**, *4*, 465−469.
(6) Bullen, C. R.; Mulvaney, P. *Nano Lett.* **2004**, *4*, 2303−2307.
(7) Beale, A. M.; van der Eerden, A. M. J.; Jacques, S. D. M.; Leynaud, O.; O'Brien, M. G.; Meneau, F.; Nikitenko, S.; Bras, W.; Weckhuysen, B. M. *J. Am. Chem. Soc.* **2006**, *128*, 12386−12387.
(8) Jensen, H.; Bremholm, M.; Nielsen, R. P.; Joensen, K. D.; Pedersen, J. S.; Birkedal, H.; Chen, Y. S.; Almer, J.; Sogaard, E. G.; Iversen, S. B.; Iversen, B. B. *Angew. Chem., Int. Ed.* **2007**, *46*, 1113−1116.
(9) Daniel, M.; Astruc, D. *Chem. Rev.* **2004**, *104*, 293−346.
(10) Storhoff, J. J.; Elghanian, R.; Mucic, R. C.; Mirkin, C. A.; Letsinger, R. L. *J. Am. Chem. Soc.* **1998**, *120*, 1959−1964.
(11) Bond, G. C.; Thompson, D. T. *Catal. Rev.—Sci. Eng.* **1999**, *41*, 319−388.
(12) Jana, N.; Peng, X. *J. Am. Chem. Soc.* **2003**, *125*, 14280−14281.
(13) Ne, F.; Testard, F.; Zemb, T.; Grillo, I. *Langmuir* **2003**, *19*, 8503−8510.
(14) Weiss, T. M.; Narayanan, T.; Wolf, C.; Gradzielski, M.; Panine, P.; Finet, S.; Helsby, W. I. *Phys. Rev. Lett.* **2005**, *94*, 038303.
(15) Panine, P.; Finet, S.; Weiss, T. M.; Narayanan, T. *Adv. Colloid Interface Sci.* **2006**, *127*, 9−18.
(16) Andreescu, D.; Sau, T. K.; Goia, D. V. *J. Colloid Interface Sci.* **2006**, *298*, 742−751.
(17) Kimling, J.; Maier, M.; Okenve, B.; Kotaidis, V.; Ballot, H.; Plech, A. *J. Phys. Chem. B* **2006**, *110*, 15700−15707.
(18) Guinier, A.; Fournet, G. *Small-Angle Scattering of X-Rays*; Wiley: New York, 1955.
(19) Glatter, O. In *Small-Angle X-ray Scattering*; Glatter, O., Kratky, O., Eds.; Academic Press: London, 1982.
(20) Spalla, O. In *Neutrons, X-rays and Light : Scattering Methods Applied to Soft Condensed Matter*; Lindner, P., Zemb, T., Eds.; Elsevier: New York, 2002; Chapter 3, pp 49−72.
(21) Gribble, G. W. *Chem. Soc. Rev.* **1998**, *27*, 395−404.
(22) Sugimoto, T. *Adv. Colloid Interface Sci.* **1987**, *28*, 65−108.
(23) Talapin, D. V.; Rogach, A. L.; Haase, M.; Weller, H. *J. Phys. Chem. B* **2001**, *105*, 12278−12285.
(24) Frens, G. *Nat.—Phys. Sci.* **1973**, *241*, 20−22.

NL0707149